

Electro-optical tunable waveguide Bragg gratings in lithium niobate induced by femtosecond laser writing

W. Horn,^{1,*} S. Kroesen,² J. Herrmann,² J. Imbrock,² and C. Denz²

¹*Nonlinear Optical Lithography, Institute of Applied Physics and Center for Nonlinear Science, Correnstr. 2-4, 48149 Münster, Germany*

²*Nonlinear Photonics, Institute of Applied Physics and Center for Nonlinear Science, Correnstr. 2-4, 48149 Münster, Germany*

[*w.horn@wwu.de](mailto:w.horn@wwu.de)

Abstract: We report the fabrication of femtosecond laser-induced, first-order waveguide Bragg gratings in lithium niobate in the low repetition rate regime. Type-II waveguides are written into an x-cut lithium niobate wafer and structured periodically to achieve narrowband reflections at wavelengths around 1550 nm. Additionally, electrodes are employed to allow for electro-optic tuning of the spectral response. We demonstrate wavelength control of the central reflection peak by applying a static external electric field. A maximum shift of the reflection peak of $\Delta\lambda = 625$ pm is observed.

© 2012 Optical Society of America

OCIS codes: (220.0220) Optical design and fabrication; (130.0130) Integrated optics; (230.7370) Waveguides; (230.1950) Diffraction gratings; (160.3730) Lithium niobate.

References and links

1. G. Della Valle, R. Osellame, and P. Laporta, "Micromachining of photonic devices by femtosecond laser pulses," *J. Opt. A.-Pure Appl. Op.* **11**, 013001 (2009).
2. J. Burghoff, C. Grebing, S. Nolte, and A. Tünnermann, "Efficient frequency doubling in femtosecond laser-written waveguides in lithium niobate," *Appl. Phys. Lett.* **89**, 081108 (2006).
3. M. Heinrich, A. Szameit, F. Dreisow, S. Döring, J. Thomas, S. Nolte, A. Tünnermann, and A. Ancona, "Evanescent coupling in arrays of type II femtosecond laser-written waveguides in bulk x-cut lithium niobate," *Appl. Phys. Lett.* **93**, 101111 (2008).
4. J. Thomas, M. Heinrich, P. Zeil, V. Hilbert, K. Rademaker, R. Riedel, S. Ringleb, C. Dubs, J. Ruske, S. Nolte, and A. Tünnermann, "Laser direct writing: Enabling monolithic and hybrid integrated solutions on the lithium niobate platform," *phys. status solidi (a)* **208**, 276–283 (2011).
5. K. M. Davis, K. Miura, N. Sugimoto, and K. Hirao, "Writing waveguides in glass with a femtosecond laser," *Opt. Lett.* **21**, 1729–1731 (1996).
6. K. Miura, J. Qiu, H. Inouye, T. Mitsuyu, and K. Hirao, "Photowritten optical waveguides in various glasses with ultrashort pulse laser," *Appl. Phys. Lett.* **71**, 3329–3331 (1997).
7. H. T. Bookey, R. R. Thomson, N. D. Psaila, A. K. Kar, N. Chiodo, R. Osellame, and G. Cerullo, "Femtosecond laser inscription of low insertion loss waveguides in Z-Cut lithium niobate," *IEEE Photon. Technol. Lett.* **19**, 892–894 (2007).
8. A. H. Nejadmalayeri and P. R. Herman, "Ultrafast laser waveguide writing: lithium niobate and the role of circular polarization and picosecond pulse width," *Opt. Lett.* **31**, 2987–2989 (2006).
9. Y. Liao, J. Xu, Y. Cheng, Z. Zhou, F. He, H. Sun, J. Song, X. Wang, Z. Xu, K. Sugioka, and K. Midorikawa, "Electro-optic integration of embedded electrodes and waveguides in LiNbO₃ using a femtosecond laser," *Opt. Lett.* **33**, 2281–2283 (2008).
10. G. D. Marshall, R. J. Williams, N. Jovanovic, M. J. Steel, and M. J. Withford, "Point-by-point written fiber-Bragg gratings and their application in complex grating designs," *Opt. Express* **18**, 19844–19859 (2010).
11. G. D. Marshall, M. Ams, and M. J. Withford, "Direct laser written waveguide-Bragg gratings in bulk fused silica," *Opt. Lett.* **31**, 2690–2691 (2006).

12. H. Zhang, S. M. Eaton, J. Li, and P. R. Herman, "Femtosecond laser direct writing of multiwavelength bragg grating waveguides in glass," *Opt. Lett.* **31**, 3495–3497 (2006).
13. H. Zhang, S. M. Eaton, J. Li, A. H. Nejadmalayeri, and P. R. Herman, "Type II high-strength bragg grating waveguides photowritten with ultrashort laser pulses," *Opt. Express* **15**, 4182–4191 (2007).
14. H. Zhang, S. M. Eaton, and P. R. Herman, "Single-step writing of bragg grating waveguides in fused silica with an externally modulated femtosecond fiber laser," *Opt. Lett.* **32**, 2559–2561 (2007).
15. G. D. Marshall, P. Dekker, M. Ams, J. A. Piper, and M. J. Withford, "Directly written monolithic waveguide laser incorporating a distributed feedback waveguide-Bragg grating," *Opt. Lett.* **33**, 956–958 (2008).
16. D. Grobnic, S. Mihailov, C. Smelser, F. Genereux, G. Baldenberger, and R. Vallee, "Bragg gratings made in reverse proton exchange lithium niobate waveguides with a femtosecond IR laser and a phase mask," *IEEE Photon. Technol. Lett.* **17**, 1453–1455 (2005).
17. J. Burghoff, S. Nolte, and A. Tünnermann, "Origins of waveguiding in femtosecond laser-structured LiNbO₃," *Appl. Phys. A* **89**, 127–132 (2007).
18. J. Burghoff, H. Hartung, S. Nolte, and A. Tünnermann, "Structural properties of femtosecond laser-induced modifications in LiNbO₃," *Appl. Phys. A* **86**, 165–170 (2006).
19. V. Apostolopoulos, L. Laversenne, T. Colomb, C. Depeursinge, R. P. Salath, M. Pollnau, R. Osellame, G. Cerullo, and P. Laporta, "Femtosecond-irradiation-induced refractive-index changes and channel waveguiding in bulk Ti³⁺:Sapphire," *Appl. Phys. Lett.* **85**, 1122–1124 (2004).
20. J. Burghoff, C. Grebing, S. Nolte, and A. Tünnermann, "Waveguides in lithium niobate fabricated by focused ultrashort laser pulses," *Appl. Surf. Sci.* **253**, 7899–7902 (2007).
21. G. J. Edwards and M. Lawrence, "A temperature-dependent dispersion equation for congruently grown lithium niobate," *Opt. Quant. Electron.* **16**, 373–375 (1984).
22. M. Ams, G. Marshall, D. Spence, and M. Withford, "Slit beam shaping method for femtosecond laser direct-write fabrication of symmetric waveguides in bulk glasses," *Opt. Express* **13**, 5676–5681 (2005).
23. G. Brown, R. R. Thomson, A. K. Kar, N. D. Psaila, and H. T. Bookey, "Ultrafast laser inscription of bragg-grating waveguides using the multiscan technique," *Opt. Lett.* **37**, 491–493 (2012).
24. N. Sanner, N. Huot, E. Audouard, C. Larat, J. Huignard, and B. Loiseaux, "Programmable focal spot shaping of amplified femtosecond laser pulses," *Opt. Lett.* **30**, 1479–1481 (2005).

1. Introduction

Fabrication of functional waveguide elements in bulk optical materials by nonlinear absorption of femtosecond radiation offers many benefits for prototyping integrated optical devices. One of the most attractive aspects of femtosecond fabrication is the feasibility to produce three-dimensional structures in a single step process by translating the host material under the laser focal point to fabricate complex networks of photonic structures, see reference [1] and therein. The inscription of three-dimensional structures especially in lithium niobate (LiNbO₃) with its nonlinear properties enables a variety of integrated optical devices such as frequency converters, evanescent couplers, and modulators [2–4].

On the one hand, waveguiding has been demonstrated in various types of silica glasses [5,6] but also crystalline materials such as LiNbO₃ [3,4,7,8] with electro-optic properties, which has been used for signal modulation in directly written, integrated Mach-Zehnder modulators [9]. On the other hand, there has been an increasing interest in periodic refractive index changes embedded into waveguides that exhibit spectral frequency selectivity comparable to in-fiber Bragg gratings which are extensively used in signal processing and sensing. Femtosecond laser-induced grating structures offer a high degree of freedom with respect to the fabrication of grating superstructures, chirps and phase-defects [10] without the need for conventional phase-mask translation since all design parameters can be programmed directly. Pointwise written Bragg gratings in waveguides have already been demonstrated in bulk fused silica glass using direct laser writing [11–14], however their reconfiguration is restricted to slow thermal or stress-based tuning [15].

In this paper we demonstrate integration of first-order, sub-surface waveguide gratings in an x-cut LiNbO₃ wafer resulting in narrowband reflections at arbitrary frequencies around 1550 nm. By integrating waveguide gratings in LiNbO₃, the grating can be reconfigured by an applied external electric field. Electro-optically shifting the central design wavelength by a

uniform electric field distribution along the grating is demonstrated.

2. Femtosecond modifications in lithium niobate

Until now, waveguide Bragg gratings (WBGs) in LiNbO₃ fabricated with infrared femtosecond pulses have only been demonstrated using phase-mask inscription into proton exchanged surface waveguides [16]. However, laser written point-by-point or burst written WBGs are desirable to enable three-dimensional, frequency selective devices but have not been realized so far due to the high degree of control over the focus to obtain regular subwavelength structures [4]. In contrast to femtosecond inscription of WBGs in fused silica a permanent and thermally stable refractive index change can only be realized by fs-pulses with energies higher than 300 nJ. Low energy pulses produce only volatile index changes (referred to as type-I modifications) exhibiting a reduced nonlinearity in the modified areas [17] whereas in fused silica high quality type-I waveguides can be easily fabricated by inscription of single tracks. However, if high energy pulses are employed to produce a stable refractive index change in LiNbO₃, the refractive index is reduced and no waveguiding can be achieved in the focal area but rather in the adjacent regions. The mechanism that leads to the higher refractive index is believed to be compensation of the stress-induced densification in the focal area [17, 18] which has also been observed in other materials e.g. Ti-doped sapphire [19]. To enable guiding with a mode matched waveguide diameter a (double-line) type-II waveguide can be produced where guiding is observed in a high index region in between two lines with reduced refractive index [20]. Fabricating a refractive index change with a narrowband reflection therefore requires a larger degree of control since the birefringence of the crystal gives rise to an anisotropic index change. The resulting stress field is intrinsically asymmetric and two pointwise tracks must be inscribed with a jitter much smaller than the periodicity itself to produce a single reflection peak. Phaseshifts between two consecutively written tracks can produce undesired passbands inside the reflection spectrum. Additionally, it is crucial to balance between the necessary stress field to achieve monomode guiding at 1550 nm which requires a minimum spacing and therefore a certain pulse energy to overlap two adjacent stress fields and to simultaneously resolve subwavelength periods without producing voids in the crystalline lattice.

3. Fabrication of WBGs

The experimental setup for fabrication and characterization of the Bragg grating waveguides is schematically depicted in Fig. 1(a). Commercially available, optical grade x-cut LiNbO₃ wafers with a thickness of 0.5 mm are placed on an x-y-z translation stage (Aerotech) and balanced to less than a micrometer with respect to the beam propagation direction. To induce the refractive index change a Ti:Sapphire femtosecond laser system (Coherent Legend) at $\lambda = 800$ nm wavelength, 120 fs pulse length, and a 1 kHz repetition rate is used delivering a total output energy up to 1 mJ. At first the pulses are picked and attenuated and subsequently focussed by a 100 \times microscope objective with a NA of 0.9 under the surface of the wafer. The pulse polarization direction is linear and parallel to the translation direction and the c-axis is aligned perpendicular to the waveguide direction. The writing process uses a feedback loop of the position synchronous output of the translation stage position encoder to trigger the synchronisation and delay generator of the regenerative amplifier. Thus positioning accuracy is significantly increased and allows for precise integration of synchronized refractive index voxels if two grating lines are written consecutively.

Lithium niobate wafers are sliced to 10 \times 10 mm² pieces using high energy femtosecond pulses. Subsequently, coupling facets are polished to optical quality. Two waveguide lines are written into the sample at a depth of 250 μ m to produce type-II waveguides in the transverse writing geometry. The distance between waveguide lines is adjusted from 7 μ m to 15 μ m to

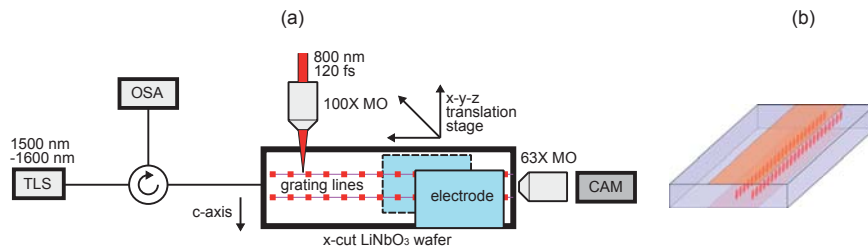


Fig. 1. Schematic experimental setup (a). Type-II waveguide gratings are written transversal and perpendicular to the *c*-axis. The samples are butt-coupled to a tunable laser source or a broadband emitting diode and read out in reflection through a circulator. The near field mode profiles are imaged from the back facet by a microscope objective. MO: microscope objective, TLS: tunable laser source, OSA: optical spectrum analyzer, CAM: InGaAs camera; Schematic representation of a WBG consisting of two modulated tracks forming a type-II WBG (b).

support sufficient guiding at 1550 nm with one or both guiding line consisting of separated refractive index voxels with a periodicity of a first order grating. This is schematically depicted in Fig. 1(b) for a grating with two modulated track. The repetition rate to fabricate continuous waveguides was 1 kHz with a translation speed of 30 $\mu\text{m/s}$ to achieve a large overlap of refractive index voxels produced by a single laser pulse. The waveguides are written with a pulse energy of 400 nJ to 600 nJ and a total length of 10 mm. First-order Bragg gratings are fabricated with center wavelengths around 1550 nm and a reduced pulse repetition rate of 100 Hz to increase writing stability due to the reduced translation velocity. To achieve different central wavelengths, the translation velocity is matched to the repetition rate [12] according to $\lambda_B = 2n_{\text{eff}} \cdot \Lambda = 2n_{\text{eff}} \cdot v/f_{\text{rep}}$ where f_{rep} is the pulse repetition rate and v the translation velocity. With an effective refractive index $n_{\text{eff}} = 2.2166$ [21] and a target wavelength $\lambda_B = 1550$ nm the translation velocity is $v = 0.03496$ mm/s for a repetition rate of $f_{\text{rep}} = 100$ Hz. This corresponds to a physical period of $\Lambda = 349.6$ nm.

To characterize the guiding properties and the spectral response, a broadband diode (Covega SLD1005) or a swept laser system (HP8168E) are used with a spectrum analyzer (HP71450B). The sample is butt-coupled to a cleaved SMF28e fiber with an index matching fluid at the tip. Due to the high index mismatch between the fused silica fiber core and the LiNbO₃ sample, the coupling surface and the fiber tip is slightly angled during the polishing to reduce unwanted interference from reflections. The probe light is polarized perpendicular to the *c*-axis of the crystal wafer and the beam propagation direction (s-polarized), whereas p-polarization refers to probe light polarized parallel to the *c*-axis as indicated in Fig. 2(a). The spectrum of the waveguide grating is read out in reflection through a circulator. Near field mode output profiles are recorded in transmission with a 63 \times microscope objective imaged onto an InGaAs camera to characterize the waveguiding properties. To enable dynamic filter reconfiguration, the sample is enclosed by copper electrodes from the top and bottom face of the wafer and connected to a high voltage power supply unit. The electrodes are separated by 500 μm and the electric field is aligned perpendicular to the crystal *c*-axis to achieve an electro-optic response.

4. Guiding properties and reflectivity of WBGs

Figure 2(a) shows an optical microscope image of waveguide input facet of two guiding lines with 15 μm spacing and Fig. 2(b) the near field mode in transmission at 1550 nm wavelength for s-polarized light. Below 7 μm spacing the type-II waveguide was not able to sustain a guided mode. Waveguiding properties strongly depend on the focussing parameters and pulse energy

employed. Monomode waveguiding was observed up to a line spacing of $25\ \mu\text{m}$, although scattering loss increased significantly. The imaged mode field exhibits an elliptical profile with 20% circularity due to the inhomogeneous distribution of the region with positive refractive index change which is accompanied by self-focussing and filamentation. More circular waveguides were observed for a higher energy with increased line spacing, however, the reflectivity of the WBG significantly decreased and higher modes can be observed. In general, guiding properties of fabricated type-II waveguide gratings using two consecutive scans per line are inferior due to the asymmetric refractive index distributions in the core compared to WBGs in fused silica fabricated in the same experimental setup using slit beam shaping [22]. It should be remarked that guiding was observed at type-II line separations down to $7\ \mu\text{m}$ which is notably narrower than published by Burghoff et.al [20] and can be attributed to the smaller numerical aperture used in the experiment. Employing a comparable numerical aperture of 0.6, the lower limit of the line spacing for waveguiding was $12\ \mu\text{m}$. However, using such a low NA, first order grating periods can not be resolved completely and the reflectivity could not be clearly observed.

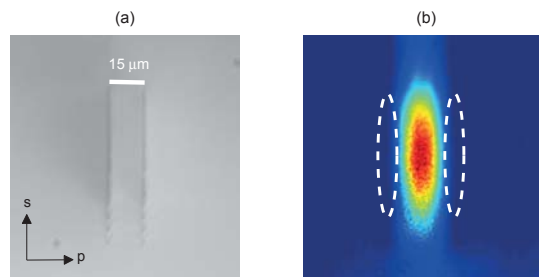


Fig. 2. Front face microscope image of the waveguide with a line distance of $15\ \mu\text{m}$ (a). Near field mode output in transmission at $1550\ \text{nm}$ wavelength with a drawn overlay of the laser modification (b).

Figure 3 shows the reflection spectra of consecutively written gratings with a pulse energy of $450\ \text{nJ}$ for both the guiding line and the grating with design wavelengths from $\lambda_B = 1530\ \text{nm}$ to $\lambda_B = 1555\ \text{nm}$. The reflectivity of the central reflection peak without boundary losses ranges from 4% to 6%. The grating reflectivity exhibits a strong dependence with respect to the input polarization state. The maximum reflectivity achieved so far was 18% with a pulse energy of $450\ \text{nJ}$ and $250\ \text{nJ}$ for the waveguide and grating line, respectively. However, in this case the reflection spectrum exhibits significantly higher background noise and sidelobes. The central reflection peak of all gratings exhibits a wavelength offset of $\Delta\lambda_B = 3.141\ \text{nm}$. This deviation is mainly due to the local increase of the refractive index and suggests $n_{\text{eff}} = 2.2211$. The spectral width is between $\Delta\lambda = 800\ \text{pm}$ and $\Delta\lambda = 1400\ \text{pm}$ depending on the pulse energy. This bandwidth range is significantly larger than the theoretical selectivity which can be as small as $\lambda_{\text{BW}} = \lambda^2 / (n_{\text{eff}}L) \approx 0.1\ \text{nm}$. We attribute this to distortions of the periodicity caused by the stress field compensation, since WBGs in fused silica fabricated in the same setup under similar conditions exhibited bandwidths of around $100\ \text{pm}$ with strong Bragg resonances ($> 10\ \text{dB}$).

By systematically testing various writing geometries, power regimes and line spacings, waveguiding and Bragg reflection was observed in various configurations. In comparison, z-cut LiNbO_3 wafers only showed p-polarized guiding and reflectance characteristics. However, in x-cut wafers where the structure was oriented perpendicular to the c-axis, only guiding of s-polarized light was observed. X-cut wafers, where the waveguide direction was parallel to the c-axis, supported guiding and Bragg reflection for both p- and s-polarized light confirming that

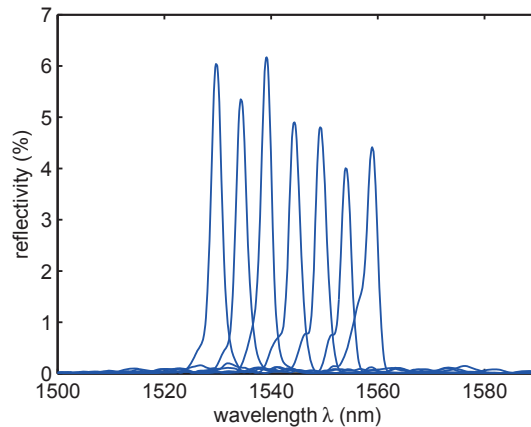


Fig. 3. Grating reflection spectra for different design wavelengths and s-polarized input light. One grating and one guiding line was written into 250 μm depth using a pulse energy of 450 nJ.

within the experimental parameters the ordinary refractive index modulation was substantially larger than the extraordinary index change.

5. Electro-optic tuning of WBGs

Figure 4 depicts the shift of the central wavelength by an external electric field for a WBG written in 100 μm depth with a spacing of 7 μm and a pulse energy of 550 nJ. The field strength is increased stepwise from -22 to +22 V/ μm . The behavior shows the expected linear

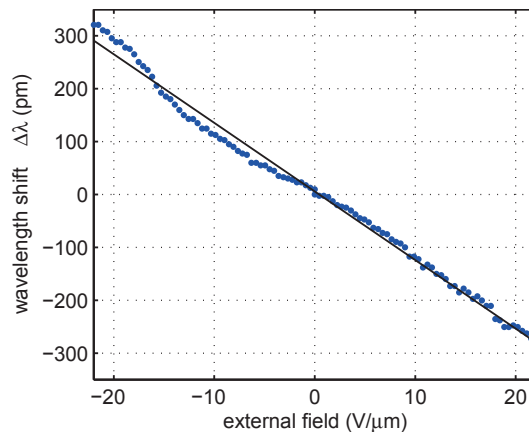


Fig. 4. Electro-optic tuning of the central reflection maximum by an applied external electric field normalized to the central reflection wavelength without the external field. The effective electro-optic coefficient $r_{\text{eff}} = 3.69$ pm/V was calculated from linear regression (solid line).

shift of the central reflection maximum. The induced refractive index offset shifts the central wavelength according to $\Delta\lambda = 2(n + \Delta n_{\text{EO}})\Lambda$ and yields an overall shift of $\Delta\lambda = 625$ pm which is about one half width of reflection maxima. The electro-optic coefficient is determined by $\Delta n = 0.5n_o^3 r_{\text{eff}} E = r_{\text{eff}} n_o^3 U / (2d)$, where U is the applied voltage over the distance d . A linear

fit yields an electro-optic coefficient of $r_{\text{eff}} = 3.69 \text{ pm/V}$.

Even though the material properties are strongly modified under intense femtosecond radiation, the electro-optic response is sufficiently preserved to control the reflection spectrum of a directly written integrated Bragg waveguide structure. In general a significantly larger electro-optic response can be obtained if the r_{33} coefficient could be employed yielding larger wavelengths shifts at comparably smaller electric fields. However, this requires sufficiently strong p-polarized guiding which has not been observed in this particular experimental realization. Further improvement may be obtained by employing multiscan methods [23] or diffractive beam shaping [24].

6. Conclusion

In conclusion we have fabricated multi-wavelength, type-II Bragg gratings around 1550 nm in lithium niobate wafers. In addition we demonstrated electro-optic control of the Bragg reflection by an external electric field. Even though the reflection spectra exhibit moderate extinction and loss properties compared to WBGs in fused silica, spectral reconfiguration by an external electric control with possibly structured electrodes offers many benefits for sensing and filtering applications.

Acknowledgments

We acknowledge support by Deutsche Forschungsgemeinschaft and Open Access Publication Fund of University of Muenster.